Steady State Experiments on High Performance, Current Profile Control and Long Sustainment of LHCD Plasmas on the Superconducting Tokamak TRIAM-1M

H. Zushi, S. Itoh, K. Nakamura, M. Sakamoto, K. Hanada, E. Jotaki, Y. D. Pan [1)],
M. Hasegawa, S. Kawasaki, H. Nakashima

Advanced Fusion Research Center, Research Institute for Applied Mechanics,
Kyushu University, Kasuga 816-8580, Fukuoka, Japan

e-mail contact of first author: zushi@triam.kyushu-u.ac.jp

1) On leave from Southwestern Institute of Physics, 610041, China

Abstract TRIAM-1M (R_0 =0.8 m, a×b=0.12 m×0.18 m and B = 8T) has the main mission to study the route toward a high field compact steady state fusion reactor. We have advanced steady state operation (SSO) programme in tokamaks, studied a heating mechanism for the high ion temperature (HIT) mode with an internal transport barrier, obtained an enhanced current drive (ECD) mode in an extended (higher power and higher density) operation regime, performed current density profile control experiments using multi-current drive systems and investigated effects of wall recycling, wall pumping and wall saturation on particle control. In HIT mode a hysteresis relation between T_i and n_e is found to be ascribed to different timescales for T_i and n_e to change. Excitation of plasma waves corresponding to ion heating is studied by both measurements of electromagnetic and electrostatic waves and their analysis. Achieved plasma parameters in ECD are as follows; n_e is 4.3×10^{19} m^{-3}, I_{LHCD} is ~ 70 kA, T_e and T_i are 0.8 keV and 0.5 keV, respectively, and the stored energy is 1.9 kJ. The energy confinement time τ_E of 8 -10 ms, $H_{ITER89\text{-}P}$ ~ 1.4, is achieved and the current drive efficiency $\eta_{CD}= \overline{n}_e I_{CD} R_0/P_{LH}$ reaches ~ 1×10^{19} A m^{-2}/W at B = 7 T under the fully non-inductive condition. Power threshold and hysteresis nature are studied. Bi-directional current drive and superposed current drive experiments have been carried out. In the former steady current reduction and peaking of j(r) are observed, but it is noticed that self-organization of j(r) occurs above a certain power ratio. In the latter broadening of j(r) can be obtained by increasing superposed RF power, however, self-organization of j(r) also occurs again at a certain power. Temporal behaviour of the recycling coefficient with two different time constants (~ 3 s and ~30 s) is analysed. The wall pumping rates are evaluated to be ~1.5×10^{16} atoms/s/m^2 for low n_e and ~4×10^{17} atoms/s/m^2 for high n_e, respectively. In the high power and high density experiments, the wall saturation phenomenon affects the density control.

1. Introduction

SSO of the high performance plasma is a crucial issue for a fusion reactor. Although there are several subjects for SSO, one of the important issues is how to maintain the high performance plasma stably for the sufficiently long period. For this purpose both physics and technological sophisticated control are required. In figure.1, the discharge duration τ_d is plotted against the magnetic field of various tokamaks. In superconducting tokamaks TRIAM-1M and Tore Supra, fully non-inductive discharge duration (two minutes ~ two hours = 10^3 τ_E ~ 10^6 τ_E) has already been achieved [1,2]. Long duration sustainment of high performance is aimed at higher power level in both devices. On the other hand, for inductive discharges, the L-mode plasma has been sustained for 60 s = 160 τ_E in JET [3]. Recent progress is found that the τ_d of the high performance plasma is extended up to 50 τ_E [4-7]. A burning duration in ITER-FEAT is 400 s and 100 τ_E, which should be further extended to the order of > 10^3 τ_E in DEMO reactor.
The physics and operational aspect for SSO relate to process taking place over several timescales, τ_E, heating time τ_{heat}, effective particle confinement time τ_p*, resistive current diffusion time $\tau_{L/R}$, wall recycling time $\tau_{recycle}$ and thermal equilibration time $\tau_{thermal}$ among plasma facing

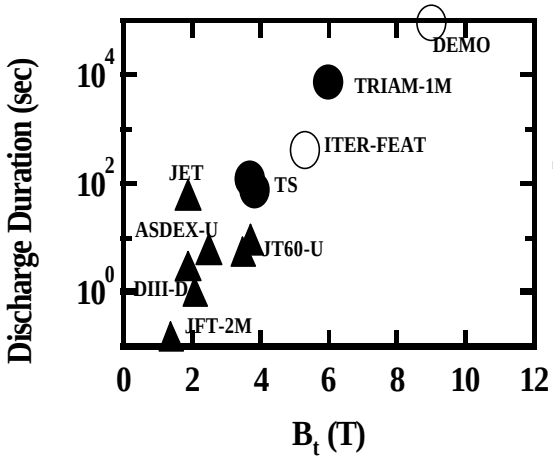

Fig.1 The discharge duration is plotted against the magnetic field in various tokamaks.

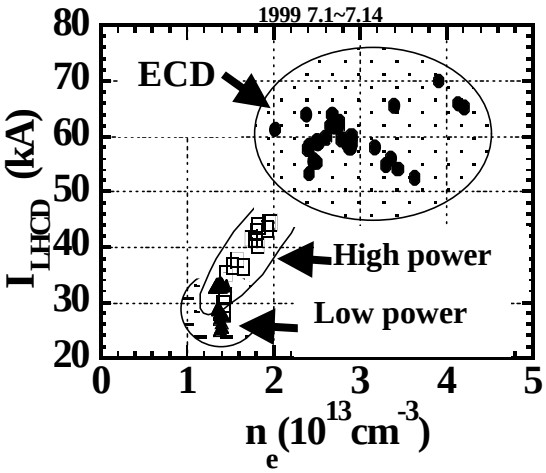

Fig.2 The extension of SSO region is plotted in the current - density plane at the high field of 7T with increasing the current drive power.

components. In burning plasmas τ_{heat} is considered to be alpha particle slowing down time and τ_p* effective He confinement time. Generally speaking, if the process approaches a stationary state with a time constant τ as 1- exp(-t/τ), the required discharge duration is ~3 τ and it is enough if we are interested in how the plasma approaches the stationary state. Thus, the discharge duration of 3 $\tau_{L/R}$ is the minimum required value for investigation of the high performance plasma associated with the current density profile, but it is not the case if this phenomenon has a threshold. In a fusion reactor the circulating power should be minimized. In this sense the threshold power P_{th} above which the high performance can be attained should be minimized and if possible, the hysteresis power window should be wide. The latter may support the idea that once the high performance state is obtained when $P > P_{th}$, this can be sustained even if $P \sim P_\alpha < P_{th}$, here P_α is the alpha particle power.

Since the last IAEA conference in Yokohama in 1998 TRIAM-1M has continued to address major issues for SSO. The following items have been carried out to understand and advance SSO scenario; a) realization of high performance including high confinement capability and enhanced current drive efficiency in a fully non-inductive plasma, b) establishment of current profile controllability and long sustainment of an optimised one, and c) understanding wall recycling, wall pumping and wall saturation during the long discharge. Since the current drive system at 8.2 GHz was installed in 1999, high power (~ 400 kW) current drive experiments have been carried out. In figure 2, the extension of the SSO range in TRIAM-1M is shown. A new current drive system was not only useful to extend the SSO region, but also essential to find a new favourable high performance mode, called enhanced current drive ECD mode. Using three current drive systems (two 8.2 GHz systems and one 2.45 GHz system of 50 kW) flexible experiments for current density profile modification and sustainment have been conducted. In the last two years TRIAM-1M has: developed plasma performance at high magnetic field of 7 T and understanding the physics of the plasma with an internal transport barrier, called HIT mode [8-10]; challenged to control the current density profile and to sustain an optimised one for long duration; and investigated and evaluated the role of the plasma facing components on the plasma density control.

This paper is conducted as follows; a brief description of the lower hybrid waves in TRIAM-1M is given in Section 2. High performance study will be presented in Section 3. Control of current profile will be demonstrated and discussed from the plasma self-organization point of view in Section 4. The dynamics of wall effects of recycling, pumping and saturation is shown in Section 5. A summary is given in Section 6.

2. Description of Lower Hybrid Waves in TRIAM-1M

2.1 LHCD plasma and system hardware

For current drive both 2.45GHz and 8.2 GHz lower hybrid current drive LHCD systems have

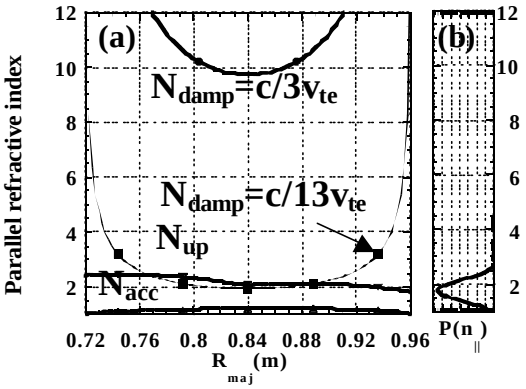

Fig.3 Characteristic parallel refractive indices, (a) N_{acc}, N_{up}, N_{damp} are plotted as a function of R_{maj}. $n_e(r)$ and $T_e(r)$ are parabolic, and squared parabolic j(r) is used. Typical experimental values and B=7 are chosen. (b) The launched $N_{||}$ spectrum for 8.2 GHz LHCD launcher is also shown.

been used. The plasma minor radius a_p is ~ 0.12 m and the major radius R_0 is 0.84 m The working gas is hydrogen. The magnetic field is 6-7 T. Two sets of the 8.2 GHz system having 8 klystrons of 25 kW each are separated toroidally by 180°. The grill type of antenna is used and the antenna phasing $\Delta\Phi$ is also scanned by the phase shifter from 70° to 270°, but most data are taken at 90°, whose peak parallel refractive index $N_{||peak}$ is ~ 1.65 corresponding to resonant electron energy of 100 keV. The spectrum is shown in Fig. 3(b). The 2.45GHz system is located between them and delivered power is ~ 30 kW. Four waveguide type grill antenna launched waves whose $N_{||peak}$ is ~ 1.8 and $\Delta\Phi$ can be varied on shot to shot basis.

2.2 Characteristics of LHW

For 8.2 GHz LHW there is no lower hybrid resonance point in the entire plasma because of $B_0 \leq 8$ T. Under these experimental conditions the ratio of 8.2 GHz to the calculated lower hybrid resonance frequency is 4-10. The launched LHW can penetrate into the whole region because of high B_t and high frequency. The critical refractive index N_{acc} (bottom line) for accessibility does not affect the wave propagation, because $N_{||peak} > N_{acc}$[11]. The up-shifting of LHW refractive index N_{up} (second thick line from the bottom) is caused by the toroidal effects, but the maximum value of N_{up} is limited to ~ 2, because of high aspect ratio of 7 and high q (>8) operation. Thus the phase velocity of the up-shifting wave is about 13 times larger than the electron thermal velocity v_{te} ($N_{damp} \sim c/13v_{te}$). In this sense there exists a large 'spectral gap' between them [12]. For 2.45GHz there are also no linear mode conversion points (corresponding to $n_{LMC} \sim 1.8\times10^{20}$ m^{-3} at B = 6T) and these waves can penetrate into the center of the plasma under the experimental conditions in Section3.1. Direct ion heating via mode conversion of LHW cannot be expected.

3. High Performance Study

3.1 High Ion Temperature HIT mode with ITB

The HIT mode is characterized by the following observations [8-10]; the density window for the onset condition, optimised antenna phasing, effective ion heating and the formation of a steep ion temperature gradient in the core regime. In this experimental campaign the effects of RF power on the width of the HIT density window and the correlation of the electromagnetic and electrostatic waves with ion heating are mainly investigated. Rf power is varied from 15 kW to 30 kW and the results show that the higher edge of the window is expanded from ~

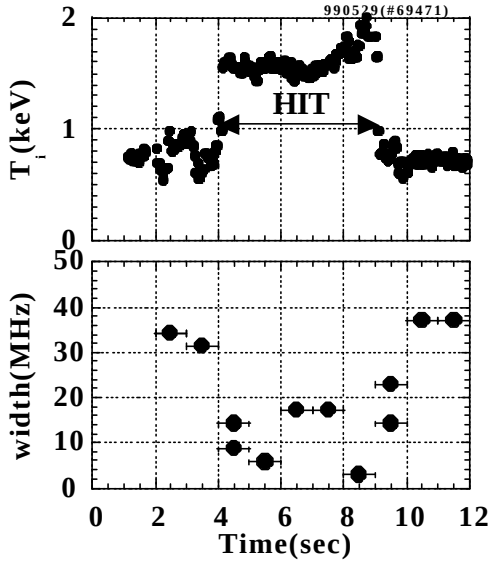

Fig.4 Time evolution of T_i and spectral width of the first lower sideband. Spectra are taken every 1 s.

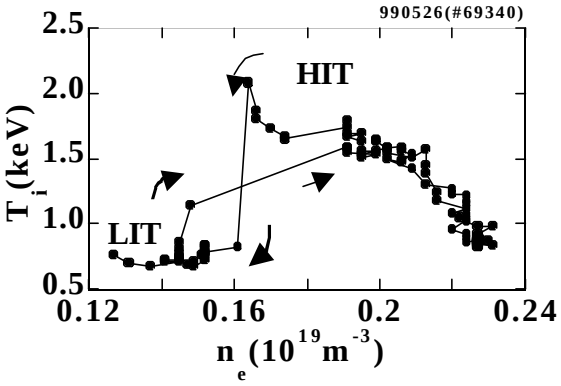

Fig.5 Hysteresis of T_i with respect to n_e at the lower edge of the HIT density window. The time trajectory of T_i is plotted as a function of n_e. Ti starts at lower n_e edge but decreases higher n_e edge of the n_e window.

2×10^{18} m^{-3} at 15 kW to ~ 2.7×10^{18} m^{-3} at 30 kW, but the lower edge is remained almost constant of ~ 1.6×10^{19} m^{-3}. In addition to the electromagnetic emission measurement outside the plasma through the quartz window, electrostatic waves are detected by Langmüir probe located at the bottom of the chamber. Both observed spectra below 3 GHz are very similar and are characterized by several satellites whose frequency separation from 2.45GHz is the ion plasma frequency. A clear correlation between narrowing of the satellites line width and ion heating is observed, as shown in Fig. 4. Although the central line density jumps up at the HIT transition by 30 %, an internal transport barrier for $n_e(r)$ is not confirmed experimentally because of the limited number of chords. The $n_e(r)$ deduced from the measured line density profile shows that the total density is increased by about 10 to 30 % in the HIT mode with keeping a relative similar profile. It should be noted that the global particle confinement property deduced from a ratio of the total number density to the H_α intensity is improved by more than 30 % in the HIT mode. Figure 5 shows a clear hysteresis characteristic of T_i around the lower edge of the HIT density window. At the higher edge of the window T_i seems to change smoothly as the density changes, however, T_i jumps in going from LIT to HIT mode or drops in going from HIT to LIT at the lower edge of the density window. Since the density profiles are different for each mode, this hysteresis may relate to a profile effect and different characteristic timescales for T_i (faster) and density (slower) at the transition.

Since the direct ion heating by LHW is not expected under these conditions, we consider ion heating mechanisms by waves excited in a low density LHCD plasma [10,13,14]. So far observed wave emissions have three distinct characteristics, (1) satellites at f = 2.45GHz ± $n\times f_{pi}$, (2) narrowing the spectral width at the HIT mode, and (3) similarity of both electromagnetic and electrostatic spectra, where f_{pi} is the frequency around the ion plasma frequency or lower hybrid frequency.

First, the satellites are only observed below ~ 6×10^{18} m^{-3}. The form of the sideband envelope shows a maximum near n= -1 to -3. In contrast with the ion cyclotron sideband spectra [15], it is very difficult to find the harmonics at f = 2.45GHz ± $n\times f_{ci}$, where f_{ci} is the ion cyclotron frequency which is ~76 MHz at the launcher position and 90 MHz at $R=R_0$. Secondly, the width Δf of sidebands is very sensitive to the HIT/LIT performance, as shown in Fig. 4. Here Δf is defined as the full width at –10 dB below the peak amplitude of the first lower sideband. It is found that Δf becomes narrow (several MHz to less than 15 MHz) in the HIT mode and in-

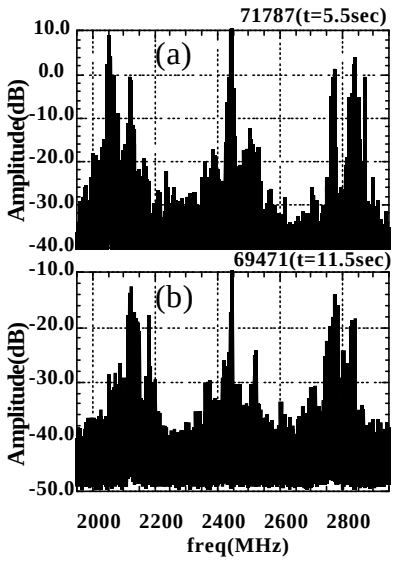

Fig.6 Spectra of floating potential of the probe in the SOL (a) and RF emission outside the plasma by a horn antenna (b). 2.45GHz is the pump LHW.

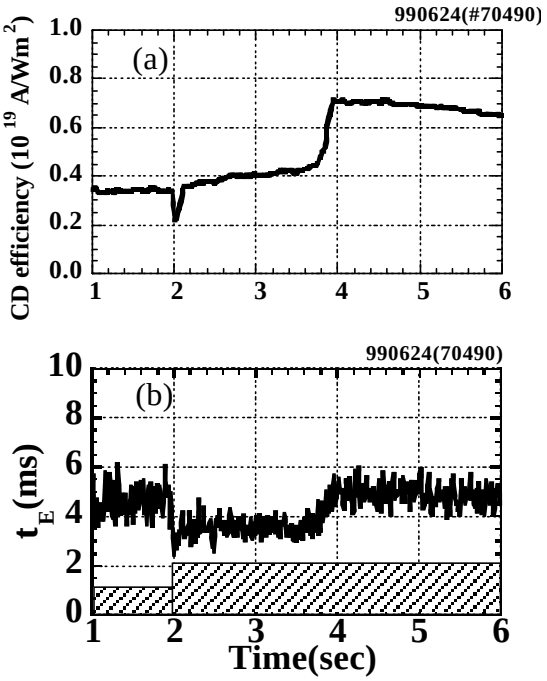

Fig.7 Enhancement of η_{CD} (a) *and* τ_E (b*) in the ECD. Hatched area indicates the waveform of RF power. At t=2 s power is increased from 65kW to 130 kW.*

creases up to 70 MHz in the LIT mode. Reduced fluctuation is a plausible explanation for the spectral narrowing and ion transport improvement [15-17]. Thirdly, similarity between both emission spectra (fig.6) suggests that waves are actually exited in the plasma core region because of its frequency corresponding to the central f_{pi}. In order to investigate waves observed at f_{pi} a reflectometry with a frequency sweepable oscillator is in preparation for local fluctuation measurement.

3.2 Enhanced Current Drive (ECD) mode

A new operation regime is found in high power 8.2 GHz LHCD plasmas [18,19]. ECD regime is clearly separated in $n_e - I_{LHCD}$ plane, as shown in Fig.2. Achieved parameters in ECD are as follows; η_{CD} is 0.9-1×10^{19} Am^{-2}/W and τ_E is 8-10 ms. η_{CD} is higher a factor of two higher than the empirical scaling and $H_{ITER89\text{-}P}$ is ~1.4. I_{LHCD} is 70 kA and the density is 4.3×10^{19} m^{-3}. Total plasma energy including the high energy component reaches ~ 2 kJ at launched rf power of 230 kW. The ion and electron temperatures are 0.5 keV and 0.9 keV, respectively. The antenna phasing is -90° whose peak $N_{\parallel}$ is ~ 1.6. The ECD regime is characterized by simultaneously improvement of η_{CD} and τ_E. In Fig. 7 it is shown that both η_{CD} and τ_E are abruptly enhanced at t ~ 3.8 s under the constant power. When rf power is increased at t = 2s, τ_E is reduced from 5 ms at 65 kW to 3.5 ms at 130 kW, indicating that the typical L-mode power law of $P^{-0.5}$ is consistent with this case. However, at t = 3.8 s such confinement deterioration is improved and τ_E is recovered. η_{CD} behaves in a different manner but it is also increased when the ECD regime is triggered. At the ECD transition both T_e and T_i, and n_e are increased. The long sustainment for this ECD regime is tried and the sustainment of this quasi steady state for 12 s (> 50 $\tau_{L/R}$) is achieved.

It should be noticed that the onset of the ECD regime is delayed by a time delay τ_{delay} after power is increased. In order to assess τ_{delay} and to investigate how this ECD regime is triggered and established the power dependence of ECD is studied. It is found that there is a certain

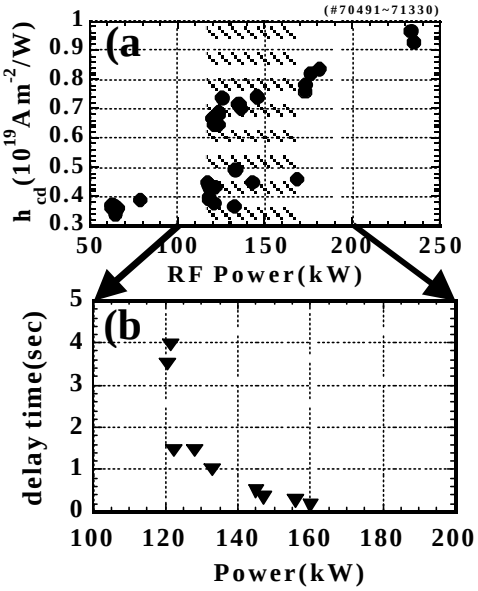

Fig.8 (a) h_{CD} versus P_{LH} . In the hatched area plasma has two values of h_{CD} during a pulse width. (b) t_{delay} decreases with increasing P_{LH}.

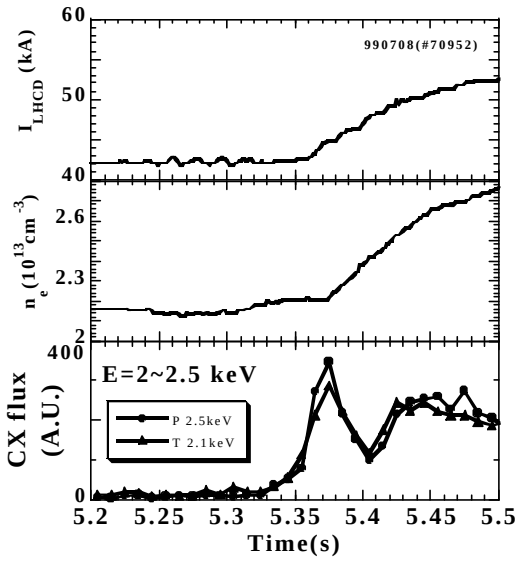

Fig. 9 I_{LHCD},, n_e and charge exchange fluxes are plotted in an expanded time-scale around the onset of ECD.

threshold power P_{th} level and hysteresis relation of η_{CD} for the ECD regime. The threshold power is ~ 130 kW at B = 7T and is ~ 1/3 of that evaluated from ITER H-mode power scaling law [20]. At P_{th} the typical value of τ_{delay} is ~ 1.5 s, which is 7 to 15 times longer than $\tau_{L/R}$, and with increasing power above P_{th} τ_{delay} becomes ~ 180 ms, which is almost the same order of $\tau_{L/R}$. Actually we consider a threshold window of power associated with τ_{delay}, as shown in Fig.8. In Ref. [21] it has been pointed out for H-mode that time constants longer than τ_E play a role in some cases for which power is close to P_{th}. However, for ECD this time delay is found in the timescale of $\tau_{L/R}$ or more. It is speculated that during the time delay the current density profile grows very slowly and triggers the onset of ECD. Power sweep experiment during a single shot also shows a clear hysteresis curve between η_{CD} and power, which is considered to link to τ_{delay}. The ratio of hysteresis power width ΔP_{th} to the averaged $<P_{th}>$ is ~ 27 %, which is a figure of merit for saving the power to sustain SSO of ECD.

Parameter changes at the onset time t_{ECD} of ECD are studied in detail. Figure 9 shows variations of I_{LHCD}, $\bar{n}_e$ and charge exchange fluxes Φ_{cx} at the energy of ~ 2 – 2.5 keV at the transition t_{ECD} denoted by the vertical line. Both perpendicularly (circles) and tangentially (triangles) measured fluxes with respect to the toroidal filed are shown. The density rise is delayed by ~ 15 ms. Since H_α intensity and the scrape-off density drop at $t = t_{ECD}$, ECD transition looks like H-mode transition. However, there is a clear difference in preceded rise of Φ_{cx}, that is, T_i. Although fast continuous T_e measurement has not been performed, a preceded rise of T_e is expected because direct ion heating due to LHW is impossible and collisional heating is only a mechanism to heat ions. Thus improved energy confinement properties in LHCD plasma trigger the density and current rise at the same power level, that is, enhancement of η_{CD}. Further investigation is under way.

In TRIAM-1M a pure non-inductive current drive experiment with a large spectral gap have been performed without toroidal induced electric field. According to the favourable $<T_e>$ dependence of η_{CD} empirical formula [22,23], when $<T_e>$ is increased from 0.2 keV to 0.3 keV,

the enhancement factor for η_{CD} is derived ~ 1.7, which is consistent with our observations. Thus the enhancement of Te leads to increase I_{LHCD} and then the I_{LHCD} increase improves the plasma performance. This positive feedback mechanism is considered for this ECD regime. However this seems not to well explain a mechanism in filling the wide spectral gap. The knocked-out cold electrons via collision with energetic electrons may play a role to fill this gap. The observed density dependence of η_{CD}, which may enhance the source particles in the gap, is studied from this point of view in Ref. [24].

Reduction of the lost energetic electrons may also enhance η_{CD}. In the ECD phase the transport of fast electrons carrying the plasma current might be improved by the same mechanism as that for bulk electrons is improved. The temperature rise ΔT_L of the limiters is measured and is compared between ECD discharges and non-ECD discharges. ΔT_L is increased with a constant of proportionality, ~0.18 ºC /kW, as the rf power is increased. In case of the ECD discharge above the threshold power ΔT_L is reduced by more than 5ºC suggesting that the lost power is reduced by 30 kW if the constant of proportionality is not affected.

4. Current Profile Control and Plasma Self-Organization

4.1 Bi-directional Current Drive Experiments

In order to increase the fraction of the bootstrap current, poloidal beta should be increased. Bi-directional current drive is one of methods to obtain such a high beta poloidal plasma [25,26]. Furthermore this method is useful to obtain a hollow current profile if the current compensation takes place near the center. On the other hand when the current compensation occurs near the edge, the current profile might become peaking. It is worth while investigating controllability for the current profile. Thus experiments using two identical 8.2 GHz systems which launch the opposite (forward FW and backward BW) traveling waves are conducted.

Target plasma whose current direction is clockwise is sustained by FW waves. The BW waves are injected into the target plasma. Both the antenna phasing are –90º (FW) and +90º (BW), respectively. The FW power P_{FW} is fixed during the discharge pulse but the BW power P_{BW} is varied shot by shot and is kept constant for the

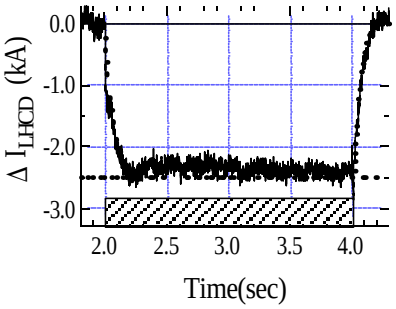

Fig.10 ΔI_{LHCD} is plotted. Dotted curves with time constant of 70 ms well fit for falling (PBW is turned on) and rising phase(turned-off). Hatched area indicates the BW injection pulse.

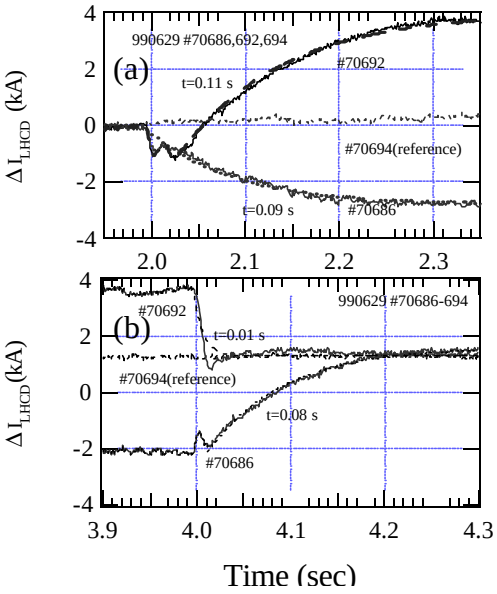

Fig.11 ΔI_{LHCD} for P_{BW}=27 kW (#70686) and 57 kW (#70692) is plotted during turn-on (a) and turn-off (b) phases.

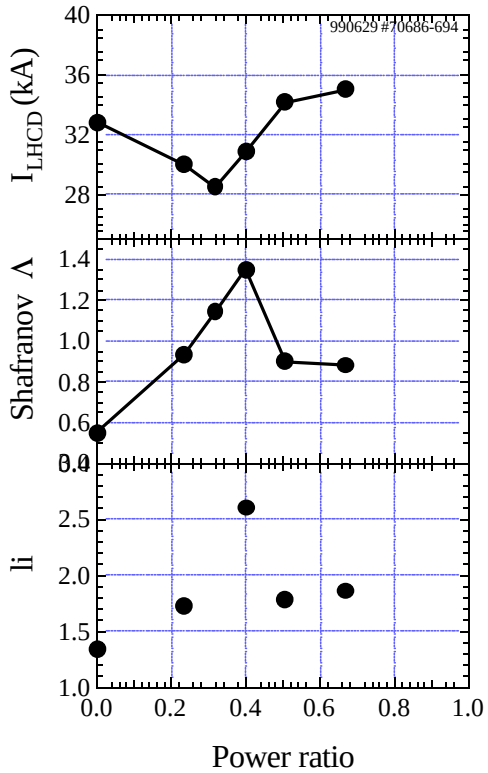

Fig.12 I_{LHCD}, Λ and l_i are plotted as a function of P_{FW}/P_{BW}.

injection duration (usually 2 s). In other case it can be swept continuously in a single shot. It is observed that I_{LHCD} is clearly reduced when P_{BW} is low, as shown in Fig.10. A relative current change ΔI_{LHCD} (= I^{FW}- I^{FW+BW}) is modelled by $\Delta I(t) = \Delta I(t_{start})(\exp(-t/\tau)-1)$ for the falling phase and by $\Delta I(t)= \Delta I(t_{end})\exp(-t/\tau)$ for the rising phase. They can well reproduce the trend of ΔI_{LHCD} (t) with a time constant of the order of $\tau_{L/R}$. The ratio $\Delta I_{LHCD}/ I_{LHCD}$ is about -10 % at the BW/FW power ratio of ~25 %. However, when P_{BW} is increased above 27 kW, the further current reduction is suppressed, and then above ~ 34 kW the direction of the total driven current is completely reversed, that is, the direction becomes the same as that driven by FW waves. Thus bi-directional current drive scenario shows a highly non-linear behaviour with respect to P_{BW}. In addition to enhancement of the FW current drive efficiency with increasing P_{BW}, temporal evolution of current cannot be reproduced by above simple exponential forms, as shown in Fig.11. This is not caused by changes of bulk plasma parameters. Changes in n_e, T_e, and T_i are small but reduced by 5-10 %. $\tau_{L/R}$ is almost unchanged.

It is observed that the number of photons at 80 keV corresponding to almost the resonant energy is increased with increasing P_{BW}, which is consistent with the increase in the stored energy. From the energy spectrum the maximum energy is also increased as P_{BW} is increased. The horizontal hard X ray profile shows that a remarkable change occurs, that is, the profile is changed from a bell shaped one (FW) to a broad or hollow one (FW+BW). It is also noted that the profile shows an in-out asymmetry, especially near the outer edge the counts are a factor of three higher than that in the FW plasma.

In order to monitor the current profile change Shafranov $\Lambda(= \beta_P+l_i/2-1)$ is measured as a function of the BW power. Here β_P is poloidal beta including the tail component β_P^{tail} and l_i is the internal inductance. These are evaluated from measured Λ and an assumption of $\beta_P^{tail} \sim C_f I_A/I_{LHCD}$ [27]. Here I_A is Alvén current and C_f is a numerical factor of order unity but actually spatial sum of X ray counts ratio to the FW only case is used. Since the hard X ray profile is not so much changed except the case of only FW, the ratio of β_P^{tail} to β_P^{bulk} is within a factor of two. The result is shown in Fig. 12. During the current compensation phase j(r) becomes peaking, while it suddenly changes to a broader one above a certain power ratio. This non-linear aspect is reproduced in a single shot during which P_{BW} is varied smoothly in time from 5 kW to ~ 70 kW for 3 s. This profile change corresponds to the enhanced forward current drive regime, that is, I^{FW+BW} is increased from initial I^{FW}.

Although the observed counter current drive scenario shows a non-linear behaviour depending on the current compensating BW power, the following explanations are considered. Since pitch angle scattering causes the perpendicular energy increase, energetic trapped electrons are produced. These electrons are drifting back and forth along their fat banana orbits, that is, when they are drifting in the BW-direction, resonant interaction occurs between BW waves and these trapped electrons. This results in detrapping the barely trapped energetic electrons in the backward direction and therefore, the backward current is produced [28]. Thus the total current

$I_{tot}= I_{FW}-I_{BW}$ is reduced. The $\eta_{CD}^* \equiv \frac{\bar{n}_e I_{LHCD} R}{P_{FW} - P_{BW}}$ is slightly increased from 0.45 (FW) to 0.5 (FW+BW) when $P_{BW} < 40$ kW. In this case P_{BW} is subtracted from P_{FW}. Since trapped particles are located in the low field side ($R > R_0$), observed in-out asymmetry in hard X ray profile can be explained by this mechanism. Furthermore it is expected that since I_{BW} tends to flow in the outer region and current cancellation is expected there, the final current density profile will become peaked. This is supported by enhancement of l_i. However, when P_{BW} is increased, the electric field should be produced via Ohm's law $E = \eta (J_{tot}-J_{BW})$, where η is the hot electron resistivity. Even though E is much small compared with Dreicer field, acceleration effects by this field cannot be neglected. In ref. [29] it is indicated that close collisions and acceleration lead to 'avalanche-like' runaway production. This assists filling the spectral gap and then enhances the forward current drive efficiency [30]. In fact η_{CD}^* increases up to 1.3 at P_{BW} of 60 kW. If the electric field is created in the outer region where the backward current is produced, enhanced forward current will selectively flow in this region. This speculation may explain l_i reduction as P_{BW} increases. Explanations for long sustainment of the enhanced forward current drive are left for the future.

4.2 Superposed current drive experiment and plasma self-organization

Using two different lower hybrid waves current profile control experiments have been carried out [31,32]. Both launched spectra have peakes at $N_{\parallel} = 1.7$ for 2.45 GHz and 1.5 for 8.2 GHz waves, respectively. A target plasma was sustained for 5 s by 8.2 GHz LHW of 80 kW and then 2.45GHz LHW of 18 kW was superposed from t = 5 s to 10 s, as shown in Fig.13. Since the direction of both waves is the same, the current increases from 20 kA to 28 kA with a time constant of 200 ms ~ $\tau_{L/R}$. Shafranov Λ drops from 1.2 to 0.6 indicating a change of the current profile because the bulk plasma parameters are not changed. The hard X-ray profile shows a change from a peaked one during the 8.2 GHz only phase to a broad one near the central reagin during the superposed phase. This observation qualitatively agrees with a change in Λ and j(r). This apparent stationary state continues for 2.5 s ~ 12 $\tau_{L/R}$. After that a self-organization phenomenon with respect to j(r) occurs suddenly. Current drops by 7 % and Λ increases up to unity. Hard X ray profile shows again the peaked profile. Other plasma parameters, n_e increases by 29 % and T_i by 10 %. The potential difference corresponding to the poloidal component of the electric field in the SOL enhances by ~ 100% and extreme enhancement of energetic charge exchange flux viewing at the bottom of the plasma. The ion toroidal drift direction is downward. No enhancement of the flux along the mid plane and at the top of the chamber is observed. These indicate that LHW coupled to electrons sustaining a performance (confinement and current drive) is changed abruptly and some part of LHW directly couple to escaping energetic ions.

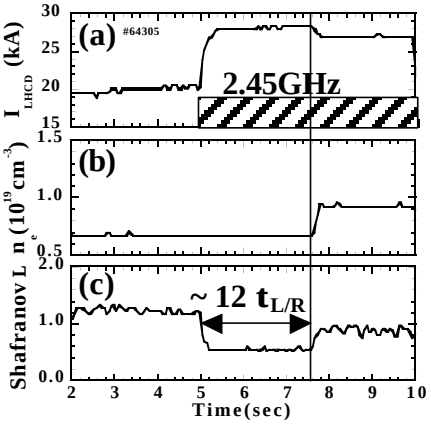

Fig. 13 Temporal changes in I_{LHCD}, n_e, and Λ are plotted during the superposed phase. After a quasi-stationary state for ~ 12 $\tau_{L/R}$, current reduction, density increase and Λ enhancement are observed under the constant superposed RF power.

The reason is not resolved why this self-organization occurs in SSO phase lasting for more than 10 $\tau_{L/R}$. However, observations presented in Section 4.1 and 4.2 give warning about knowledge for SSO associated with current profile obtained during a short period less than 10 $\tau_{L/R}$. In a SSO plasma j(r) can be modified by plasma itself with a time delay.

5. Wall Recycling, Wall Pumping and Wall Saturation

In order to control the plasma density in SSO it is quite important to know how the recycling coefficient R and the wall-pumping rate behave during the discharge [33,34]. This subject is investigated in long duration discharges under the all-metal environment with molybdenum Mo limiters, Mo divertor plates and stainless steel wall without low Z material coating. The experimental conditions are as follows: The RF power of 2.45 GHz LHW is ~ 20 kW and that of 8.2 GHz LHW is ~ 300 kW. The line averaged electron density is 0.1- 0.2×10^{19} m^{-3} for 2.45 GHz plasma and 1-3 $\times10^{19}$ m^{-3} for 8.2 GHz plasma. Figure 14 shows time evolution of R (t) in 2.45 GHz and 8.2 GHz LHCD plasmas. R (t) seems not to depend on n_e in this range and there exist two time constants of a few seconds and several tens of seconds for R (t). Since the outflux to the wall monitored by ion saturation current and CX flux are constant in time, these two time constants may reflect processes on the wall itself, that is, physical adsorption, implantation, diffusion of hydrogen atoms in the material and desorption.
Physical adsorption may reach an equilibrium state and desorption progresses with a shorter time constant, but the implanted energetic ions accelerated in the sheath near the wall or bombarded energetic CX neutrals take a longer time for release from the surface.
The assessment of the wall pumping rate is performed both in 70 minutes for 2.45 GHz and 33 seconds for 8.2 GHz plasmas. The hydrogen gas was supplied through a piezo electric valve so as to keep the Hα line intensity at the central chord constant. First, the result is as follows for 2.45 GHz. The averaged gas feed rate from 10 to 40 min was about 1 $\times10^{17}$ atoms/s but the gas feed was automatically stopped several times during the discharge because of feedback control of gas supply. This means that the R becomes unity or more and again decreases below unity, i.e. the wall seems to repeat a process of being saturated and refreshed. The particles evacuated by an external pump-unit subtracted from the total amount of gas supply is the amount of the particles pumped by the wall, as shown in Fig.15 (a). Here the plasma density and the neutral gas pressure are kept almost constant during the discharge. The averaged wall pumping rate, which is obtained from a slope of the curve in Fig.15 (a), is about 1.5 $\times10^{16}$ atoms/s/m^2. About

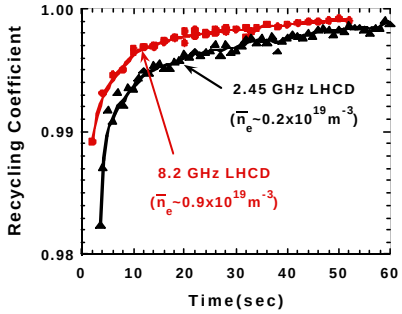

Fig. 14 Time evolution of recycling coefficients in 2.45 GHz and 8.2 GHz LHCD discharges.

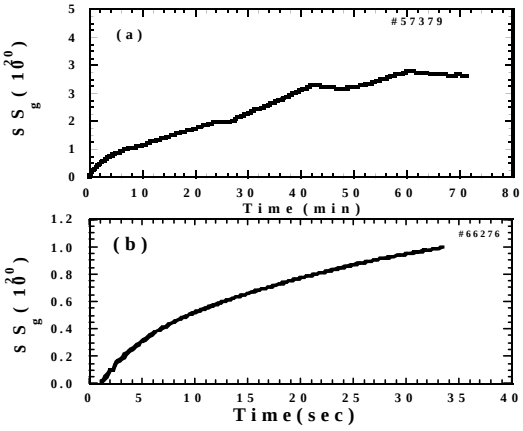

Fig.15 Total amounts of gas feed and evaluation to the external pump in 2.45GHz (a) and 8.2 GHz (b).

3×10^{20} hydrogen atoms are pumped by the wall for 70 min. Secondly, for 8.2 GHz, higher pumping rate of about 4×10^{17} atoms/s/m^2 is obtained as shown in Fig. 15 (b), but this was ~30 times in magnitude higher than that of 2.45 GHz even though the wall saturation has been already seen at lower pumping rate. This difference is not due to the initial wall conditions. We notice that the difference of CX flux blow 0.7 keV, where CX flux of 8.2 GHz is higher than that in 2.45 GHz plasma. It means that particles with relatively low energy contribute to the wall pumping. These CX neutrals damaged the wall and caused co-deposition of Mo on the wall surface [35]. This structure change of the wall surface keeps capability of the wall pumping, that is, refreshment of the wall.

6. Summary

The three major issues for SSO have been investigated in fully non-inductive plasmas at the high magnetic field (B = 6-7 T). The SSO aspects for each issue, that is, onset of the transition (several τ_E), sustainment of the improved state (>10^3 τ_E), current profile modification and self-organization (~20 $\tau_{L/R}$), wall recycling, pumping and saturation on density control ($\tau_{recycle}$, $\tau_{thermal}$) are studied on each characteristic timescale. The results are summarised below.

The operation window of the HIT could be expanded by increasing RF power. Both ion energy and particle confinement properties are enhanced during the HIT phase. The physical mechanism for ion heating in LHCD plasmas is studied and excitation of waves well corresponding to ion heating are confirmed.

A new favourable mode ECD has been achieved at the higher density (> 1.7×10^{19} m^{-3}) and higher power (> 130 kW) regime. The confinement improvement factor with respect to $\tau_{ITER89\text{-}P}$ is ~ 1.4. The power threshold for onset of the ECD and hysteresis power relation is investigated. The hysteresis power width is ~ 0.27 $P_{threshold}$. The current drive efficiency reaches twice the empirically obtained $<T_e>$ dependent scaling. The ECD occurs with a time delay once the drive power reaches the threshold value. This time delay is much longer than $\tau_{L/R}$, but it depends inversely on the RF power.

Current profile control experiments were performed using bi-directional LHW. When the current is compensated by backward travelling waves, Shafranov Λ increases monotonically with P_{BW}. Above a certain power ratio Λ drops abruptly, which indicates that a self-organization occurs on the driven current profile.

Self-organization is also observed in the superposition experiments of 2.45 GHz and 8.2 GHz LHW. Superposing the broader 2.45 GHz spectrum and varying its power it is found that the current profile is spontaneously changed from a peaked profile to a broad one. However, at some conditions, a certain power and density the current profile strongly tends to go back to the previous peaked one.

Wall recycling, wall pumping and wall saturation have been investigated using very long pulse discharges under all metal surface circumstances. The temporal evolution of the recycling coefficient has been investigated in long pulse discharges and it is found that the recycling coefficient varies with two time constants of ~ 3 s and > 30 s, respectively. Wall pumping rate has been evaluated and it is found that even once the wall pumping saturates, the wall starts to pump out the particles via refreshment of the wall surface. In high power and high density plasma wall saturation is one of the important issues to extend the discharge duration.

References

[1] ITOH, S., et al, in Fusion Energy 1996 (Proc. 16th Int. Conf., Montreal, 1996) Vol. **3,** IAEA, Vienna (1997) 351.
[2] EQUIPE TORE SUPRA, in Fusion Energy 1996 (Proc. 16th Int. Conf., Montreal, 1996) Vol. **1,** IAEA, Vienna (1997) 141.
[3] STORK, D. and the JET Team, 'Recent JET Results', JET-P(93) 33, 1993
[4] ISHIDA, S. and THE JT-60 TEAM, FUSION ENERGY **1**. (1998) 13.
[5] The JET Team, FUSION ENERGY **1**. (1998) 29.
[6] TAYLOR, T.S., et al., FUSION ENERGY **1**. (1998) 49.
[7] GRUBER, O., et al., FUSION ENERGY **1**. (1998) 213.
[8] ITOH, S., et al., Nuclear Fusion **39Y** (1999) 1257.
[9] ZUSHI, H., et al., Nuclear Fusion **39Y** (1999) 1183.
[10] ZUSHI, H, et al., Nuclear Fusion **40** (2000) 1183.
[11] STIX, T. H., 1992 Chapter 4 in 'Waves in Plasmas' American Institute of Physics New York.
[12] FISCH, N. J., Rev. of Mod. Phys. **59** (1987) 175-234.
[13] COPPI, B., et al., Nucl. Fusion **16** (1976) 309.
[14] PARAIL, V.V., High-Frequency Plasma Heating, American Institute of Physics, New York (LITVAK, A. G., Ed.) (1992) Ch. 5.
[15] TAKASE, Y., et al., Phys. Fluids **28** (1985) 983.
[16] CESARIO, R., et al., Nucl. Fusion **32** (1992) 2127.
[17] PERICOLI-RIDOLFINI, V., et al., Nucl. Fusion **34** (1994) 469.
[18] ZUSHI,H., et al., J Plasma and Fusion Research **76** (2000) (in press).
[19] HANADA, K., et al., J Plasma and Fusion Research **76** (2000) (in press).
[20] SNIPES, J. A., et al., Plasma Phys. Control. Fusion **42** (2000) A299.
[21] RYTER, F., et al., Nuclear Fusion **36** (1996) 1217.
[22] BARBATO, E., Plasma Phys. and Controlled Fusion **40** (1998) A63-A76.
[23] USHIGUSA, K., Plasma Phys. and Controlled Fusion **38** (1996) 1825-1830.
[24] HANADA, K., et al., this conference.
[25] LUCKHARD, S.C. et al., Phys. Rev. Lett. 62 (1989) 1508.
[26] MAEKAWA, T, et al., Nucl. Fusion **31** (1991) 1394.
[27] MONDELLI, A., OTT, E. Phys. Fluids **17** (1974) 1017.
[28] OHKAWA, T., General Atomic Company Report GA-A 13847 (1976).
[29] CHIU, S. C., ROSENBLUTH, M. N., HARVEY, R. W., CHAN, V. S., Nuclear Fusion **38** (1998) 1711.
[30] CHAN, V. S., PARKS, P. B., CHIU, S.C., and HARVEY, R., W., J. Plasma Fusion Res. , 1999 (in press).
[31] SAKAMOTO, M., et al., Nuclear Fusion **40Y** (2000) 453.
[32] NAKAMURA, K., et al., this conference.
[33] SAKAMOTO, M., et al., in Contrl. Fusion and Plasma Phys. (Proc. 24th Eur. Conf., 1997) Vol. 21A,PartII, European Physical Soc., Geneva (1997) 721.
[34] SAKAMOTO, M., et al, in this conference.
[35] HIRAI, T., et al., J. Nucl. Mater. **258-263** (1998) 1060.